Proceedings of NAMRI/SME, Vol. 41, 2013

Determination of Constitutive Material Model Parameters in FE-Based Machining Simulations of Ti-6Al-4V and IN-100 Alloys: An Inverse Methodology

Durul Ulutan, and Tuğrul Özel
Manufacturing Automation Research Laboratory
Department of Industrial and Systems Engineering
Rutgers University
Piscataway, New Jersey, USA

ABSTRACT
Finite Element-based simulations provide good capability to predict the outcomes of machining processes, and their value soar when utilized to simulate machining of hard-to-machine materials such as titanium alloys (e.g. Ti-6Al-4V) and nickel-based alloys (e.g. IN-100). This study presents a new FE simulation-based methodology to determine the modified constitutive model parameters utilizing the force results from face turning experiments conducted for both Ti-6Al-4V and IN-100. In these simulations, material constitutive models have a great influence on the results and must be selected carefully to represent the correct material flow stress characteristics. Conventional modified constitutive material models with flow softening behavior are utilized and further modified to represent the thermal softening effect on the flow softening behavior, where the temperatures can be much higher than normal for machining these materials. Parameters of the temperature-dependent flow softening based material constitutive model for both materials have been determined by using an inverse methodology. Comparison of measured and simulated forces with the modified material models has shown close agreements.

KEYWORDS
Flow Stress, Inverse Methodology, Finite Element

INTRODUCTION

Titanium alloy Ti-6Al-4V (Ti-64) is one of the most commonly used alloys in the aerospace, automotive, and medical device industries. It offers high strength-to-weight ratio, as well as good corrosion resistance and bio-compatibility. However, this alloy is considered to be difficult to machine due to its low thermal conductivity, elastic modulus, and diffusivity, as well as its high rigidity and chemical reactivity at elevated temperatures [1-3]. Nickel-based alloy IN-100 is also a mission-critical component material used mostly in aircraft and industrial gas turbine engines, but also difficult to machine due to its high toughness and work hardening behavior. Because of the difficulties in machining these alloys, selection of machining and tool geometry and preparation parameters is critical. Since it is very costly to experimentally discover the effects of each parameter, finite element (FE)-based simulations are relied on to illustrate the machining conditions and predict the results of the process. Therefore, it is essential to bring the capabilities of these simulations to the lowest possible error level allowed by technological constraints.

Chip formation during machining these materials has been investigated intensively by researchers [4-15], as it is different than conventional materials. Chip is typically segmented due to the adiabatic shearing mechanism in the primary shear zone, requiring special attention during analysis. Also, because of elevated temperatures during machining, flow softening is observed at higher temperatures [16-18]. In order to eliminate the very costly and time consuming nature of repeated experimentation, finite element-based simulations have been conducted mostly concerning these changes in the mechanics of the process [19-21]. In these simulations, instead of using damage (material failure) models, modified constitutive models with temperature-dependent flow softening based adiabatic shearing have been utilized to represent these characteristics. For the flow stress data, Split-Hopkinson Pressure Bar (SHPB) tests are utilized, where the original Johnson-Cook material model parameters are determined [22-27]. Sensitivity analysis on these parameters has also been conducted [28-31], but this analysis only includes the original parameters that can already be measured, or the parameters that do not belong to the flow softening

characteristics of these materials. As a result, there is a lack of methodology on determining the additional parameters brought by modifying the Johnson-Cook flow stress model, and this study aims to fill that void by proposing an inverse methodology utilizing FE-based simulations validated by experimental force measurements.

FACE TURNING EXPERIMENTS

In most of the validation studies, orthogonal machining tests are conducted and simulations in 2D are validated with the results of these experiments. However, in order to represent the mechanics of the industrial machining processes better, 3D face turning experiments were conducted. In 3D face turning experiments (see Figure 1), contrary to the orthogonal machining experiments, the cutting edge is not orthogonal to the cutting velocity. For this reason, forces in the thrust direction (F_p) are more significant compared to orthogonal machining. In the figure, depth of cut is symbolized with a_p, whereas F_c, F_f, and F_p are the cutting, feed, and thrust forces respectively, r_ε is the nose radius and r_β is the cutting edge radius of the tool. Face turning experiments were conducted to investigate the effects of different machining and tool parameters, and to determine which set of constitutive material model parameters represent the flow stress of the material the best. In these experiments, all of the cutting tools were Tungsten-Carbide/Cobalt (WC/Co) material, but some of them were coated with TiAlN coating. Three different cutting edge radii were available at 25 µm, 10 µm, and 5 µm (sharp edge), and a fourth different type of insert was available as TiAlN coated on a sharp cutting edge, providing approximately 10 µm cutting edge.

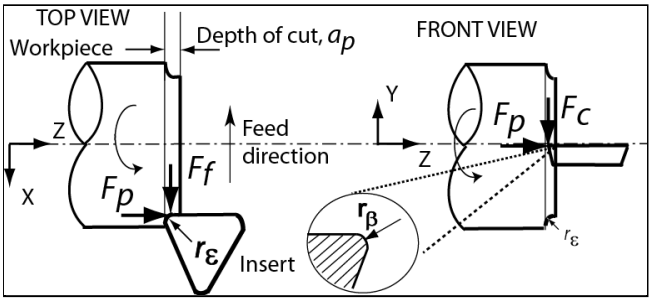

Figure 1. Configuration of face turning experiments [32].

Face Turning Experiments on Ti-64

For the machining experiments on Ti-64, a cylindrical workpiece that was 165 mm long and 100 mm in diameter was utilized to measure forces. In addition to the two different tool options (uncoated and coated), two cutting speed values were selected (v_c=55 and 90 m/min), as well as two feed values (f=0.05 and 0.1 mm). For these combinations of three variables, 8 sets of experiments were conducted at a_p=2 mm depth of cut. No cutting fluid or coolant was applied in any of these experiments, and they were run in dry cutting conditions in order to create suitable modeling conditions for experimental validation.

Face Turning Experiments on IN-100

For the machining experiments on IN-100, disks of 6-7 mm thickness prepared from a cylindrical bar were utilized for force measurements. Two cutting speed values were selected (v_c=12 and 24 m/min), and all four different types of cutting inserts were utilized. Hence, the cutting edge radius varied from r_β=5 µm to 10 and 25 µm, whereas coated and uncoated inserts were used at 10 µm cutting edge radius. In order to have more stability on the force measurements, a smaller depth of cut value of a_p=1 mm was used for all the experiments in IN-100. Similar to the Ti-64 experiments, no cutting fluid or coolant was applied in order to be able to illustrate the experimental conditions in the FE-based simulations in the best way.

FE-BASED SIMULATIONS

3D simulations (as shown in Figure 2) illustrating the face turning experiments were conducted for all experimental conditions, where the workpiece was assumed to show viscoplastic behavior. The friction conditions between the tool and the workpiece were both defined as hybrid in the rake and flank faces, and the Coulomb friction coefficients used were 0.6 and 0.5, respectively for Ti-64, and 0.7 and 0.6, respectively for IN-100 [32]. For the shear friction factor, 0.9 was used for both faces and for both materials. Approximately 50,000 elements were used to define the workpiece, and approximately 150,000 elements were used to define the tool. All the simulations were run for 2 milliseconds, which is usually more than enough for the machining process to reach steady-state conditions, and a heat transfer coefficient of 100,000 was defined (much higher than its actual value) to speed up the simulations to reach steady-state values, without affecting the results.

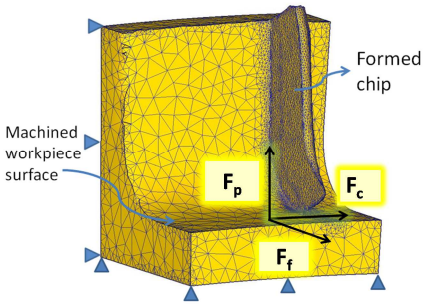

Figure 2. Representation of 3D simulations.

Constitutive Material Model

Original Johnson-Cook (JC) material model represents the flow stress (σ) of the material in terms of strain (ε), strain rate ($\dot{\varepsilon}$), and temperature (T). Using SHPB tests, the original JC material model parameters (A, B, C, n, m) can be determined (Eq. 1), where $\dot{\varepsilon}_0$ is the reference strain rate, T_0 is the ambient temperature, and T_m is the melting temperature of the material. These original JC model parameters have been determined by many researchers for different materials and many are published for Ti-64, and the ranges the values are published show that the exact parameters cannot be found [22-27]. However, the approximate range of these parameters can be observed from these findings, and investigation of parameters can be initiated from these values. From the original parameter sets, the values given in Table 1 were used for Ti-64 and IN-100. Then, starting from these values, the parameters that emerge in the modified JC constitutive material model (a, b, d, r, s) are added to represent temperature-dependent flow softening based adiabatic shearing (Eq. 2).

$$\sigma = [A + B\varepsilon^n]\left[1 + C\ln\frac{\dot{\varepsilon}}{\dot{\varepsilon}_0}\right]\left[1 - \left(\frac{T-T_0}{T_m-T_0}\right)^m\right] \quad (1)$$

$$\sigma = \left[A + B\varepsilon^n\left(\frac{1}{exp(\varepsilon^a)}\right)\right]\left[1 + C\ln\frac{\dot{\varepsilon}}{\dot{\varepsilon}_0}\right] \left[1 - \left(\frac{T-T_r}{T_m-T_r}\right)^m\right]\left[D + (1-D)\left[\tanh\left(\frac{1}{(\varepsilon+p)^r}\right)\right]^s\right] \quad (2)$$

where $D = 1 - \left(\frac{T}{T_m}\right)^d$, and $p = \left(\frac{T}{T_m}\right)^b$.

Table 1. Original Johnson-Cook material flow stress model parameters.

Alloy	*A*	*B*	*n*	*C*	*m*
Ti-64	725	683	0.65	0.035	1
IN-100	1350	1750	0.65	0.017	1.3

Chip Formation

In the Finite Element-based simulations, it is essential that the chip is formed in order to be able to illustrate the physical nature of the machining process. Hence, all simulations were run at least until the chip formation was observed (see Figure 2).

Steady-State Assumption

With Finite Element-based simulations, it is not feasible to simulate the whole machining process of few seconds. Instead, usually only the first few milliseconds of the process is simulated. However, it is known that the forces and temperatures during machining reach their steady-state values very quickly. To this end, although the whole experiment was not simulated, steady-state conditions in forces and temperatures were reached in every set of Finite Element-based simulations.

Temperatures during simulations do not reach steady state in default conditions. In order to overcome this problem and ensure that the simulations reach steady-state temperatures, a higher heat transfer coefficient than normal of 100,000 was utilized. This way, thermal loads at steady-state conditions were also successfully illustrated. While the increased heat transfer coefficient ensures steady-state conditions, it does not affect output values. Temperature-dependent mechanical and thermophysical properties of work and tool materials have been given in Table 2.

Table 2. Temperature-dependent mechanical and thermo-physical properties of work and tool materials used in FE simulations.

Property	Unit	WC/Co	Ti-6Al-4V	IN-100
E**(T)**	GPa	$5.6\cdot10^5$	$7.4\cdot10^{-4}\cdot T+113$	$-72\cdot T+217000$
α**(T)**	1/°C	$4.7\cdot10^{-6}$	$3\cdot10^{-9}\cdot T+7\cdot10^{-6}$	$1.1\cdot10^{-5}$
λ**(T)**	W/m•°C	55	$7.039\cdot e^{0.0011*T}$	$10.3\cdot e^{0.008*T}$
c_p**(T)**	N/mm²•°C	$5\cdot10^{-4}\cdot T+2.07$	$2.24\cdot e^{0.0007*T}$	$3.62\cdot e^{0.0004*T}$

METHODOLOGY TO DETERMINE PARAMETERS

Before starting the procedure to determine the modified flow stress model parameters (a, b, d, r, s), the original Johnson-Cook model parameters (A, B, C, m, n) should be determined via SHPB tests [23]. For this reason, the values in Table 1 were utilized to initiate the algorithm. 3D machining simulations were employed to represent face turning processes, and chip formation that represents steady-state results was achieved in every simulation. These simulations were designed and conducted using DEFORM 3D software. The first step to the algorithm (Figure 3) was to select meaningful values by experience for the modified JC material flow stress model parameters (a, b, d, r, s) and run initial simulations for all the machining conditions designed. Then, forces were extracted from finalized simulations, and it was verified that steady-state conditions were reached at the end of the simulations. The errors between the predicted and experimental forces were calculated and recorded for each simulation for later comparison. Different combinations of these modified model parameters were utilized to find solutions that resulted in comparable predicted steady-state forces. While selecting the different combinations of these parameters, the flow stress curve was paid attention to, because the model requires that the flow stress curve represents flow softening behavior that is dependent on temperature, while ensuring similarity with SHPB test results at low strain values.

When acceptable results were found for these parameters, it was observed that the errors could be decreased even further, so the original model parameters were considered for change. It is noteworthy to realize that *C*, and *m* represent the changes in strain rate and temperature in the original JC model, while *A* represents the flow stress at zero strain, reference strain rate, and ambient temperature conditions. Hence, these parameters should be kept unchanged to stay on the same curves of the original JC model. However, changing the other two original JC parameters (*B* and *n*) would only represent changes in the effect of strain on flow stress, which is already altered by the modified model through flow softening. Therefore, in order to improve the results even further, these values were updated within the ranges reported by different references. When the minimum force error is achieved, flow stress solution is said to be found for the material.

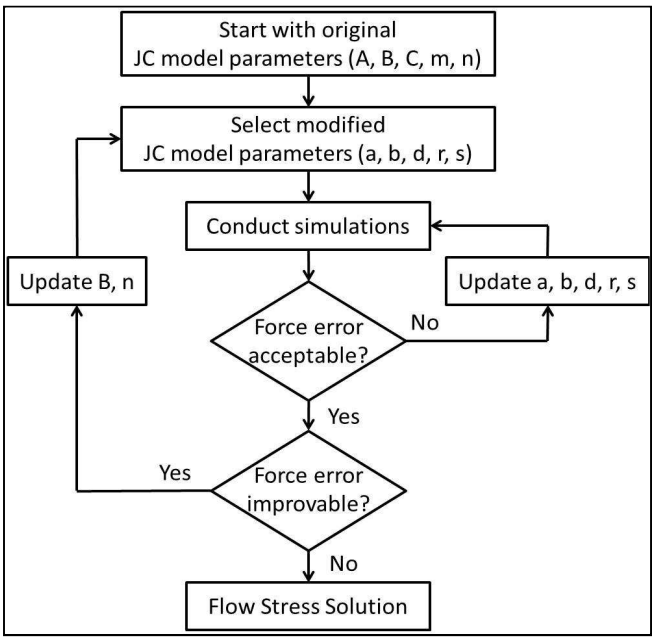

Figure 3. Flow diagram to achieve modified JC model parameters and the flow stress solution.

The calculation of the resultant error is straightforward: For the set of simulations, the difference in each force component (F_c, F_p and F_t) is calculated as a percentage. Then, the total error is calculated using Eq. (3): Each error percentage is squared, and the sum of these squares is found for each simulation and each force component. Then, this sum of squares is divided by the number of machining conditions (*M:* the number of simulations in a set) and the number of force components (*N*=2 for orthogonal machining, 3 for 3D machining simulations). The square root of this value gives the resultant force error ε_{tot}, which is utilized in comparing the accuracy of each flow stress model representation. If the error for a new set improves (decreases) the resultant force error, the new set of parameters is set as the base for the next parameter iteration. If not, the results from the previous sets are compared with the results from the new set, and the next parameter set is decided based on this comparison. In Eq. 3, $F_{i,exp}$ represents the experimental value of any of the force components (cutting, thrust, or feed directions), whereas $F_{i,sim}$ represents its simulated value.

$$\varepsilon_{tot} = \sqrt{\frac{\sum_{j=1}^{M}\sum_{i=1}^{N}\left[\left(\frac{F_{i,exp}-F_{i,sim}}{F_{i,exp}}\right)^2\right]_j}{N \cdot M}} \qquad (3)$$

RESULTS AND DISCUSSIONS

FE-based machining simulations with different sets of modified (temperature-dependent flow softening based) material flow stress model parameters were conducted for both Ti-64 and IN-100, and the resultant errors for all sets of simulations were determined. According to these resultant errors, best sets of parameters that are selected to represent flow stress of the materials are shown in Table 3.

For both Ti-64 and IN-100, these sets of parameters led to 23% resultant error in predictions. These temperature-dependent flow softening based material model parameters can be used for further simulations in similar machining conditions, but for significantly different machining conditions, these parameters should be determined again with new force measurements obtained. For these sets of parameters, force comparisons for all sets of simulations are presented in Table 4 for Ti-64 and Table 5 for IN-100 materials. These tables show experimental and simulated force results for face turning, as well as errors associated with each of the machining conditions.

It was observed that for Ti-64, the resultant error varied between 13% and 30%, but for IN-100, it varied between 11% and 40%.

The methodology is iterated in two rounds of analysis. In the first round, Johnson-Cook model parameters (*A, B, C, m, n*) were fixed, while modified model parameters (*a, b, d, r, s*) were iterated over 30 simulation rounds. In the second round of analysis, Johnson-Cook model parameters (*A, C, m*) were kept fixed, while *B* and *n* were iterated.

In order to improve these results even further, more iterations on Johnson-Cook and modified material model parameters can be done. It should be noted that each simulation round in average takes about 50 hours on a PC with Intel Core Duo microprocessor.

Table 3. Best set of modified material flow stress model parameters for both materials.

Alloy	***A***	***B***	***n***	***C***	***m***	***a***	***b***	***d***	***r***	***s***
Ti-64	725	300	0.65	0.035	1	0.5	2	0.5	12	-0.05
IN-100	1350	1750	0.65	0.017	1.3	1.5	10	0.01	1.5	-0.4

Table 4. Force comparison (simulated vs. experiments) for Ti-64 (a_p=2 mm). ε_{tot} = 23%.

				Experimental			Simulated			
Coating	r_β	v_c	f	F_p	F_c	F_f	F_p	F_c	F_f	Err
	µm	m/min	mm	N	N	N	N	N	N	%
None	25	55	0.05	324	439	117	205	519	105	24
			0.1	456	777	161	340	953	166	20
		90	0.05	288	443	114	187	468	98	22
			0.1	356	780	167	344	951	174	13
TiAlN	10	55	0.05	495	241	526	568	128	120	30
			0.1	573	387	845	1041	187	191	23
		90	0.05	330	239	470	563	117	126	20
			0.1	488	355	850	939	179	172	17

Table 5. Force comparison (simulated vs. experiments) for IN-100 (a_p=1 mm). ε_{tot} = 23%.

				Experimental			Simulated			
Coating	r_β	v_c	f	F_p	F_c	F_f	F_p	F_c	F_f	Err
	µm	m/min	mm	N	N	N	N	N	N	%
None	5	12	0.05	272	507	268	276	541	172	21
	10			290	494	208	302	583	204	11
	25			319	517	211	323	630	229	14
TiAlN	10			320	494	185	305	600	197	13
None	5	24		337	587	180	354	629	222	14
	10			245	545	201	300	566	204	13
	25			179	484	215	290	543	209	37
TiAlN	10			172	501	215	289	564	191	40

CONCLUSIONS

In this study, an inverse methodology using experimental force measurements was utilized in order to determine the modified material model parameters. 3D face turning experiments were conducted to obtain machining forces. Finite Element-based simulations were designed and conducted to illustrate these machining processes, and their results were compared to experimental findings. Different sets of parameters were employed in order to achieve the minimum error between experimental and simulated values of machining forces, and the sets of parameters that provide these minimum errors for both the titanium alloy Ti-64 and the nickel-based alloy IN-100 were determined. These sets of parameters are considered nearly the best possible sets to illustrate these machining conditions and they can be utilized in further analyses of machining effects on these hard-to-machine materials.

ACKNOWLEDGMENTS

The financial support provided by the National Science Foundation (grant number CMMI- 1130780), and the support for DEFORM software by SFTC, Ohio, USA are gratefully acknowledged.

REFERENCES

[1] Yang, X., Liu, C.R., 1999. Machining titanium and its alloys. Machining Science and Technology, 3/1: 107-139.

[2] Ezugwu, E.O., 2005. Key improvements in the machining of difficult-to-cut aerospace superalloys. International Journal of Machine Tools and Manufacture, 45: 1353-1367.

[3] Arrazola, P.J., et al., 2009. Machinability of titanium alloys (Ti6Al4V and Ti555.3)" Journal of Materials Processing Technology, 209/5: 2223-2230.

[4] Komanduri, R., Turkovich, B.F., 1981. New observations on the mechanism of chip formation when machining titanium alloys. Wear, 69: 179-188.

[5] Gatto, A., Iuliano, L., 1994. Chip formation analysis in high speed machining of a nickel base superalloy with silicon carbide whisker-reinforced alumina. International Journal of Machine Tool & Manufacture, 34/8: 1147-1161.

[6] Vyas, A., Shaw, M.C., 1999. Mechanics of saw-tooth chip formation in metal cutting. ASME Journal of Manufacturing Science and Engineering, 121/2: 163-172.

[7] Gente A., Hoffmeister, H.W., 2001. Chip formation in machining Ti6Al4V at extremely high cutting speeds. CIRP Annals, 50/1: 49-52.

[8] Molinari, A., Musquar, C., Sutter, G., 2002. Adiabatic shear banding in high speed machining of Ti-6Al-4V: experiments and modeling. International Journal of Plasticity, 18: 443-459.

[9] Cotterell, M., Byrne, G., 2008. Dynamics of chip formation during orthogonal cutting of titanium alloy Ti-6Al-4V. CIRP Annals – Manufacturing Technology, 57/1: 93-96.

[10] Li, J.L., et al., 2008. A FEM study on chip formation in orthogonal turning nickel-based superalloy GH80A. Material Science Forum, 575-578: 1370-1375.

[11] Lorentzon, J., Jarvstrat, N., Josefson, B.L., 2009. Modeling chip formation of alloy 718. Journal of Machining Processing Technology, 209: 4645-4653.

[12] Sun, S., Brandt, M., Dargusch, M.S., 2009. Characteristics of cutting forces and chip formation in

machining of titanium alloys. International Journal of Machine Tools and Manufacture, 49: 561-568.

[13] Khidhir, B.A., Mohamed, B., 2010. Study of cutting speed on surface roughness and chip formation when machining nickel-based alloy. Journal of Mechanical Science and Technology, 24/5: 1053-1059.

[14] Pawade, R.S., Joshi, S.S., 2011. Mechanism of chip formation in high-speed turning of Inconel 718. Machining Science and Technology, 15: 132-152.

[15] Siemers, C., et al., 2011. Chip formation and machinability of nickel-base superalloys. Advanced Material Research, 278: 460-465.

[16] Miller, R.M., Bieler, T.R., Semiatin, S.L., 1999. Flow softening during hot working of Ti-6Al-4V with a lamellar colony microstructure. Scripta Materialia, 40/12: 1387-1393.

[17] Ding, R., Guo, Z.X., 2004. Microstructural evolution of a Ti-6Al-4V alloy during β-phase processing: experimental and simulative investigations. Materials Science and Engineering A, 365: 172-179.

[18] Cui, W.F., et al., 2009. High temperature deformation behavior of α+β-type biomedical titanium alloy Ti-6Al-7Nb. Material Science and Engineering A, 499: 252-256.

[19] Calamaz, M., Coupard, D., Girot, F., 2008. A new material model for 2D numerical simulation of serrated chip formation when machining titanium alloy Ti-6Al-4V. International Journal of Machine Tools and Manufacture, 48: 275-288.

[20] Özel, T., Sima, M., Srivastava, A.K., 2010. Finite element simulation of high speed machining Ti-6Al-4V alloy using modified material models. Transactions of the North American Manufacturing Research Institution of SME, 38: 49-56.

[21] Özel, T., et al., 2010. Investigations on the effects of multi-layered coated inserts in machining Ti-6Al-4V alloy with experiments and finite element simulations. CIRP Annals – Manufacturing Technology, 59/1: 77-82.

[22] Lee, W.S., Lin, C.F., 1998. High-temperature deformation behavior of Ti6Al4V alloy evaluated by high strain-rate compression tests. Journal of Materials Processing Technology, 75: 127–136.

[23] Lee, W.S., Lin, C.F., 1998. Plastic deformation and fracture behavior of Ti–6Al–4V alloy loaded with high strain rate under various temperatures. Materials Science and Engineering A, 241: 48–59.

[24] Meyer, H.W., Kleponis, D.S., 2001. Modeling the high strain rate behavior of titanium undergoing ballistic impact and penetration. International Journal of Impact Engineering, 26: 509–521.

[25] Chen, L., El-Wardany, T.I., Harris, W.C., 2004. Modeling the effects of flank wear land and chip formation on residual stresses. CIRP Annals – Manufacturing Technology, 53/1: 95–98.

[26] Seo, S., Min, O., Yang, H., 2005. Constitutive equation for Ti–6Al–4V at high temperatures measured using the SHPB technique. International Journal of Impact Engineering, 31: 735–754.

[27] Li, L., He, N., 2006. A FEA study on mechanisms of saw-tooth chip deformation in high speed cutting of Ti–6–Al–4V alloy. Proceedings of the Fifth International Conference on High Speed Machining (HSM), Metz, France: 759–767.

[28] Sartkulvanich, P., Altan, T., Gocmen, A., 2005. Effects of flow stress and friction models in finite element simulation of orthogonal cutting-a sensitivity analysis. Machine Science and Technology, 9: 1–26.

[29] Martinez, A., et al., 2008. Inverse analysis methodology to determine flow stress data for finite element modeling of machining. 11th CIRP Conference on Modeling of Machining Operation, Gaithersburg, MD USA.

[30] Shatla, M., Kerk, C., Altan, T., 2001. Process modeling in machining, part I: determination of flow stress data. International Journal of Machine Tools & Manufacture, 41: 1511-1534.

[31] Özel, T., Altan, T., 2000. Determination of workpiece flow stress and friction at the chip-tool contact for high-speed cutting. International Journal of Machine Tools & Manufacture, 40: 133-152.

[32] Özel, T., Ulutan, D., 2012. Prediction of machining induced residual stresses in turning of titanium and nickel based alloys with experiments and finite element simulations. CIRP Annals - Manufacturing Technology, 61: 547-550.